

Metric-Learning based Deep Hashing Network for Content Based Retrieval of Remote Sensing Images

Subhankar Roy, *Student Member, IEEE*, Enver Sangineto, *Member, IEEE*, Begüm Demir, *Senior Member, IEEE*, and Nicu Sebe, *Senior Member, IEEE*

Abstract—Hashing methods have been recently found very effective in retrieval of remote sensing (RS) images due to their computational efficiency and fast search speed. The traditional hashing methods in RS usually exploit hand-crafted features to learn hash functions to obtain binary codes, which can be insufficient to optimally represent the information content of RS images. To overcome this problem, in this paper we introduce a metric-learning based hashing network, which learns: 1) a semantic-based metric space for effective feature representation; and 2) compact binary hash codes for fast archive search. Our network considers an interplay of multiple loss functions that allows to jointly learn a metric based semantic space facilitating similar images to be clustered together in that target space and at the same time producing compact final activations that lose negligible information when binarized. Experiments carried out on two benchmark RS archives point out that the proposed network significantly improves the retrieval performance under the same retrieval time when compared to the state-of-the-art hashing methods in RS.

Index Terms—deep hashing, metric learning, content based image retrieval, remote sensing.

I. INTRODUCTION

THE advancement of satellite technology has resulted in the explosive growth of remote sensing (RS) image archives. Such high volume of RS archives has ushered a rapid development of content-based image retrieval (CBIR) methods in RS, aiming at finding the most similar images to a given query image q . Typically, a CBIR system is split into a two-stage pipeline: (1) compute an effective representation of each image by means of its descriptor; and (2) measure the similarity between the query image and every image in the archive based upon the image descriptors.

Traditional nearest neighbor search algorithms (which exhaustively compare the query image with each image in the archive) are time consuming and thus prohibitive for large-scale RS image retrieval problems. To alleviate the high time complexity, hashing based nearest neighbour search techniques have been recently proposed in RS. Typically, hashing based methods involve learning a hash function, $l = h(x)$, which maps a high dimensional image descriptor $x \in \mathbb{R}^d$ to a very low dimensional binary code $l \in \mathbb{R}^K$, where $d \gg K$. Besides improving the computational efficiency, hashing methods also reduce the storage costs significantly. One of the most well known unsupervised hashing method is locality-sensitive hashing (LSH) [1] which learns b hash functions $[h_1, h_2, \dots, h_b]$ by choosing b random vectors obtained from a multivariate Gaussian distribution. In the context of CBIR in RS, two hashing based nearest neighbour search methods have been introduced in [2]–[4]. Demir et al. [2] adapted

to RS data properties and tested two kernel-based hashing methods that learn hash functions in the kernel space from hand crafted features, which are the most widely used bag-of-visual-words (BoVW) representations computed on the scale invariant feature transform (SIFT) features. In [3], these hashing methods have been extended to represent each image with multi-hash codes (each of which corresponds to a primitive present in the image) obtained from hand crafted features such as spectral histograms of the image regions. The effectiveness of the binary codes relies on the approach used for the hash function generation and also the considered image descriptors for which the hash functions are applied. Hand-crafted features may have limited capability to accurately represent the high level semantic content of RS images. This issue may lead to insufficient binary codes that can result in inaccurate retrieval results under complex RS image retrieval tasks.

The limitations of hand-crafted features have been overcome by the deep convolutional neural networks (CNN), which learn very effective representations of images. As an example, Li et al., [4] introduced a deep hashing neural network (DHNN) to address CBIR in RS. The DHNN jointly learns semantically accurate deep image features and binary hash codes that utilizes a cross-entropy loss to construct the cost function. While entropy based losses are particularly effective in classification problems, it fails to define a notion of separation between the similar and dissimilar images, which is essential in CBIR frameworks. The absence of a margin threshold between positive and negative samples leads to poor generalization. As a result, to achieve high retrieval performance the DHNN requires long hash codes and high amount of annotated training images, which is difficult to collect in RS archives.

To address these issues, in this letter we present Metric-Learning based Deep Hashing Network (MiLaN) that learns a semantic-based metric space, while simultaneously producing binary hash codes for fast and accurate retrieval of RS images. Differently from [4] our network provides more compact binary hash codes under identical training conditions. The contribution of this letter, which significantly extends our work presented in [5], also consists in experimental analysis on an additional large-scale benchmark archive.

II. METRIC-LEARNING BASED DEEP HASHING NETWORK

In this letter we aim to learn a hash function that encodes an image into a binary code (in the Hamming space) constructed with only 0s and 1s. In details, we assume that a small set of training images is available. We assume that a small set $\mathcal{I} = \{x_1, x_2, \dots, x_P\}$, where each x_i is associated with a

corresponding class label $y_i \in \mathcal{Y} = \{y_1, y_2, \dots, y_P\}$ is initially available and the proposed network aims to learn a hashing function $h : \mathcal{I} \rightarrow \{0, 1\}^K$, K being the number of bits in the hash code. The hash function h is learned by the MiLaN conditioning on the fact that binary codes of length K must capture the semantics of images in the metric space.

MiLaN adopts a primary loss function that, on the one hand, aims to cluster samples which are similar and separates samples that are dissimilar. This is accomplished by using a *triplet loss* [6], which learns a metric space so that the Euclidian distance between two points in the semantic space faithfully corresponds to the semantic distance between their corresponding pair of images in the pixel space. Moreover, two additional losses: 1) a representation penalty loss, which pushes the final activations of the network to be as close to 0 or 1; and 2) bit balancing loss, which aims to encourage the network to produce hash codes having equivalent number of 0s and 1s, are also considered while training. To further reduce the dependence of MiLaN on annotated training images, we include a pre-processing stage before the training stage. During this pre-processing stage, every image of the training set \mathcal{I} is fed to a pre-trained Inception Net [7] and the high level feature representation is extracted from the layer, $Pool_3$, which is right before the softmax layer. The layer $Pool_3$ comprises of the activations of 2048 neurons, which are obtained by performing average pooling on the feature maps of the layer before. Let $\mathcal{G} = \{g_1, g_2, \dots, g_P\}$, $g_i \in \mathbb{R}^{2048}$ represent the features that are extracted from the images in \mathcal{I} . \mathcal{G} is then used as input to MiLaN (see Fig. 1). We would like to point out that we do not fine-tune the Inception Net, which is a quite common practice in recognition tasks using transfer learning. Instead we simply use the pre-trained network as a feature extractor.

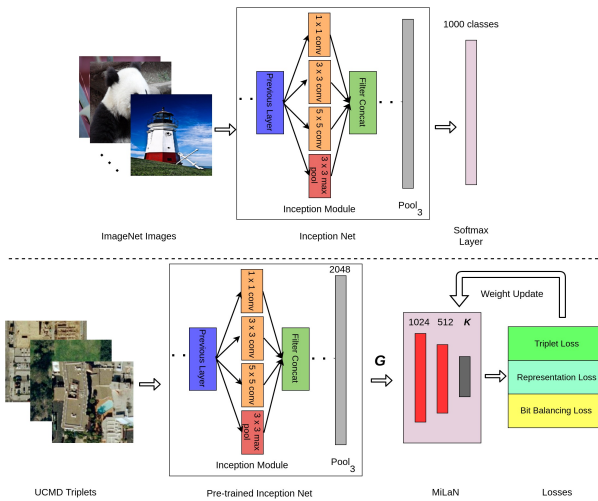


Fig. 1: Overall training pipeline. Top: Inception Net pretrained on ImageNet images. Bottom: Inception Net is used to extract an intermediate image representation, which is then fed to our MiLaN to obtain binary codes of length K .

Subsequently, the extracted features $\{\mathcal{G}\}_{i=1}^P$ are given as input to MiLaN with randomly initialized weights. MiLaN is trained to map the input feature vectors g_i into a metric space which is semantically significant such that: $f : \mathbb{R}^{2048} \rightarrow \mathbb{R}^K$.

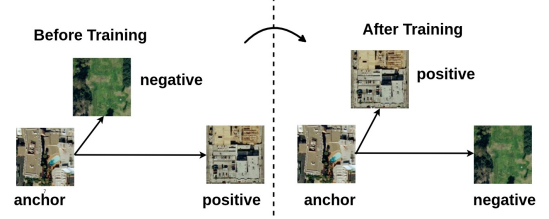


Fig. 2: The intuition behind the triplet loss: after training, a positive sample is “moved” closer to the anchor sample than the negative samples of the other classes.

The real activations of \mathbb{R}^K are then quantized using a simple thresholding to obtain the binary hash codes. The main driving loss of our MiLaN is the triplet loss which is learning the metric space. The triplet loss (see Fig. 2) is built with the intuition that images with the same label (or at least sharing visual semantics) should lie closer to each other in the metric space than the dissimilar images, which must lie farther apart. As an example, images of category “airplane” should be closer to each other in the target metric space than the images from category “baseballfield”. The triplet loss is formulated by using the class label y_i associated with X_i . More specifically, a triplet of data samples needs to be sampled from the extracted feature set \mathcal{G} . A triplet is composed of $\mathcal{T} = \{(g_i^a, g_i^p, g_i^n)\}$, where g_i^a (known as *anchor*) is sampled randomly from the set of feature vectors g_i with an associated class label y_i ; g_i^p (known as *positive*) is the feature vector associated with the same class label as g_i^a , i.e., y_i and g_i^n (known as *negative*) is again chosen randomly from \mathcal{G} such that it belongs to a class y_j , where $y_j \neq y_i$. For training the network with stochastic gradient descent (SGD) a mini-batch M of triplets \mathcal{T} is chosen with goal of minimizing the following triplet loss:

$$\mathcal{L}_{Metric} = \sum_{i=1}^M \max \left(0, \|f(g_i^a) - f(g_i^p)\|_2^2 - \|f(g_i^a) - f(g_i^n)\|_2^2 + \alpha \right), \quad (1)$$

where α is the minimum margin threshold, which is forced between the positive and negative distances. At the end of the training it is desired that the feature vector g_i^a of a specific image is closer to the feature vectors g_i^p of all other images from the same class than to any feature vector g_i^n of a different class. Therefore, the following constraint needs to be fulfilled:

$$\|f(g_i^a) - f(g_i^p)\|_2^2 + \alpha < \|f(g_i^a) - f(g_i^n)\|_2^2 \quad (2)$$

$$\forall (f(g_i^a), f(g_i^p), f(g_i^n)) \in \mathcal{T}$$

Our proposed MiLaN consists of just 3 fully-connected layers with 2 hidden layers having 1024 and 512 neurons and the final layer made of K output neurons, where K is the number of desired hash bits. We use LeakyReLU in the two hidden layers to allow negative gradients to flow during the backward pass and a sigmoid activation in the final layer to restrict the output activations between [0, 1]. In order to push the final real activations towards the extremities of the allowable range, we derive inspirations from [8] and impose

a second loss term whose goal is to maximize the sum of the squared errors between the output layer activations of MiLaN and 0.5. Notationally it can be written as:

$$\mathcal{L}_{Push} = -\frac{1}{K} \sum_{i=1}^P \|f(g_i) - 0.5\mathbf{1}\|^2, \quad (3)$$

where $\mathbf{1}$ is a vector of 1's having dimension K .

Also inspired by [8], we adopt the third loss term which forces the output neuron to fire with a 50% chance. This means that the binary code representations of the images will have a balanced number of 0s and 1s.

$$\mathcal{L}_{Balancing} = \sum_{i=1}^P (\text{mean}(f(g_i)) - 0.5)^2, \quad (4)$$

where $\text{mean}(f(g_i))$ is the mean of the output activations of the hashing network.

In sum, the final objective function is a weighted combination of the three losses given as:

$$\mathcal{L} = \mathcal{L}_{Metric} + \lambda_1 \mathcal{L}_{Push} + \lambda_2 \mathcal{L}_{Balancing}, \quad (5)$$

where λ_1 and λ_2 are the hyperparameters.

After the hashing network is trained with the combined losses, the final hashing function $h(\cdot)$ is obtained by quantizing the values in \mathbb{R}^K . For a given archive image X , from the evaluation set, the $Pool_3$ features g from Inception Net is obtained followed by applying the hash function $h(\cdot)$ to get the binary code $b = h(g)$. The quantization is done as following:

$$b_n = (\text{sign}(v_n - 0.5) + 1)/2, 1 \leq n \leq K \quad (6)$$

Finally, in order to retrieve an image X_j , which is semantically most similar to a query image X_q , we use the Hamming distance between $h(X_q)$ and $h(X_j)$. During retrieval the Hamming distance is computed between the query $h(X_q)$ and each image in the archive and the distances obtained are then sorted in ascending order of magnitude. The top- k instances with the lowest distances are retrieved.

III. DATASET DESCRIPTION AND DESIGN OF EXPERIMENTS

In our experiments we have used two benchmark RS archives. The first archive is the widely used UC Merced [9] (UCMD) archive that contains 2100 aerial images from 21 different land cover categories, where each category includes 100 images. The pixel size of each image in the archive is 256×256 and the spatial resolution is 30 cm. The second benchmark archive used for our experiments is the Aerial Image Data Set [10] (AID) which is much larger with respect to the UCMD archive. The images were extracted from the Google Earth and each image in the archive is a section of 600×600 pixels. AID contains 10000 images from 30 different categories and the number of images in each category varies between 220 to 420. The spatial resolution of images in this archive varies between 50 cm to 8 m.

MiLaN¹ was trained by choosing a mini-batch of triplets having a cardinality $M=30$. For a much larger archive we suggest to include only those triplets in the mini-batch, which

contain semi-hard negatives (only those negative samples which violate the threshold margin in (2)) for a faster convergence of the network. The value of the threshold margin α was set to 0.2, which is determined by a cross-validation. To this end a validation set of 20 images per class are used to find the optimum value of α . Hyperparameters $\lambda_1=0.001$ and $\lambda_2=1$ are also chosen with this validation set. For the loss function optimization Adam Optimizer was used with a small learning-rate $\eta = 10^{-4}$. The other two hyper-parameters β_1 and β_2 of the Adam optimizer were set to 0.5 and 0.9, respectively.

For both archives, the results of the proposed MiLaN were compared with those obtained by: 1) the Support Vector Machine (SVM) classifier applied to the SIFT based descriptors; and (2) the kernel-based supervised locality-sensitive hashing method (KSLSH) [2] that is a state-of-the-art supervised hashing method. Moreover, we compared the results with those obtained by the DHNN. However, due to the lack of availability of code of the DHNN we could report its results only for the UCMD archive. In the experiments, Gaussian RBF kernel was used for the KSLSH and the SVM. For each hashing method, the length K of the hash code (i.e., the total number of hash bits) was tested within the range of [8-64] with a step size increment of 8. Results of each method are provided in terms of: i) mean average precision (mAP); and ii) computational time. The retrieval performance was assessed on top-20 retrieved images. In the experiments, we considered two different scenarios. In the first scenario, we did not include any data augmentation and have selected 60% of images associated to each category as training images (MiLaN and in hyper-parameter selection), while the rest was considered as test images (which are used to evaluate the retrieval performance). In the second scenario, we have considered data augmentation by geometric transformations.

IV. EXPERIMENTAL RESULTS

A. Results: UCMD Data Set

In Table I we report the results of the first scenario where we compare the mAP for the top-20 retrieved images (mAP@20) and retrieval time for the SVM and the KSLSH with our proposed MiLaN when $K = 16, 24$ and 32 . As seen from Table I the MiLaN provides 33.4% better mAP than the SVM with a significantly reduced retrieval time. In addition, the proposed MiLaN for $K = 24$ yields a mAP that is 29.6% higher than the KSLSH, under similar retrieval time. Qualitative results are visually observed in Fig. 4 where for a given query image of an “airplane”, the proposed MiLaN retrieves semantically more similar images than the KSLSH. For example, the images retrieved at the 4th and 19th places (see Fig. 4b) do not belong to the category “airplane” whereas with our proposed MiLaN all the images at the corresponding positions (see Fig. 4c) belong to the same category as the query image.

We perform experiments on the UCMD archive also under the second scenario, where we consider data augmentation as suggested by [4]. Accordingly, we replicate the experimental set-up of the DHNN [4] by augmenting the original data set with images rotated by 90° , 180° and 270° , yielding 8400 images. Then, out of the 8400 images, 7400 are randomly chosen for training the network and remaining 1000 images

¹Code is available at <https://github.com/MLEnthusiast/MHCLN>

TABLE I: mAP@20 and average retrieval time for the SVM, the KSLSH [2] and the proposed MiLaN for the UCMD archive.

Methods	mAP	Time (in ms)	# Hash Bits K					
			$K=16$		$K=24$		$K=32$	
			mAP	Time (in ms)	mAP	Time (in ms)	mAP	Time (in ms)
SVM	0.556	92.3	-	-	-	-	-	-
KSLSH [2]	-	-	0.557	25.3	0.594	25.5	0.630	25.6
Our MiLaN	-	-	0.875	25.3	0.890	25.5	0.904	25.6

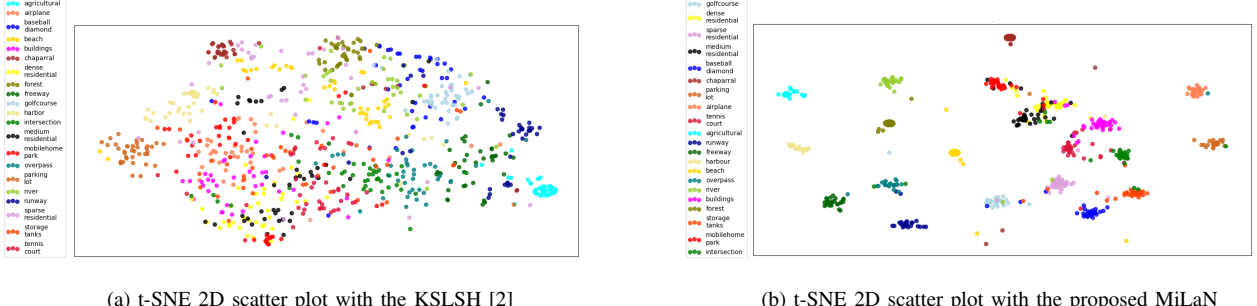
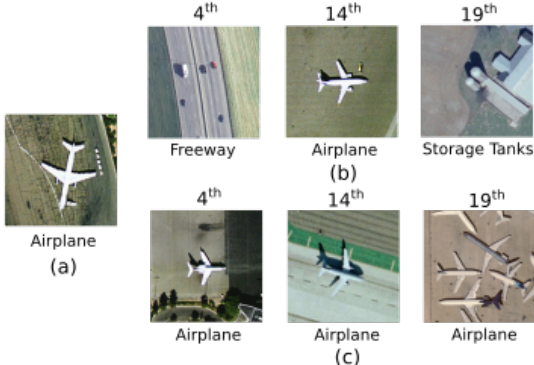
Fig. 3: t-SNE 2D scatter plots comparing the 2D-projection of K -dimensional binary hash codes of the test images in the UCMD archive. Each colour in the plot represents a land-cover category. This is best viewed in colour with maximum zoom.

Fig. 4: (a) Query image, (b) images retrieved by the KSLSH [2] and (c) images retrieved by the proposed MiLaN.

are used for evaluation. It is worth noting that 7400 training images are also used as a search set as suggested by [4]. Table II compares the mAP for the top-50 retrieved images by the DHNN [4] and our proposed MiLaN. It is observed that the MiLaN requires smaller K for reaching a higher mAP. For instance, when $K = 32$, the mAP for the MiLaN is 5.4% higher than that of the DHNN. Moreover, the mAP for the MiLaN with $K = 32$ is again 2.4% higher than the mAP obtained by the DHNN with twice the number of hash bits, i.e., $K = 64$. We would like to point that use of such experimental set-up as proposed by [4] may lead to the identical but rotated variants of a same image being present in both training and test sets and thus leading to over-saturated results. Also, the network will be prone to memorizing the test samples (rotated variants) which are present in the training set. However, we adopt this training and evaluation strategy just to fairly compare with [4].

To visualize the K -dimensional Hamming codes corresponding to test images, we perform a t-distributed stochastic

TABLE II: mAP@50 obtained by the DHNN [4] and the MiLaN with data augmentation for the UCMD archive.

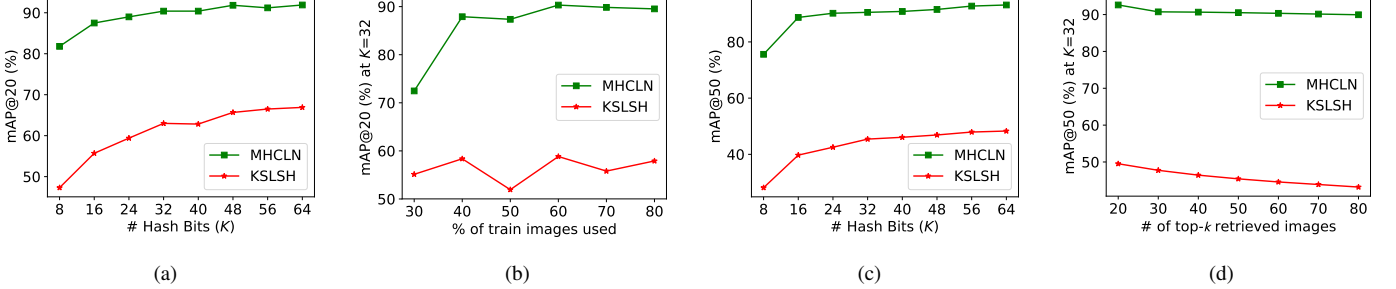
Methods	# Hash Bits K	
	$K = 32$	$K = 64$
DHNN [4]	0.939	0.971
Our MiLaN	0.993	0.995

neighbour embedding (t-SNE) by projecting them to 2D. As we can visually observe in Fig. 3a, even though the samples of the “agricultural” category stand out clearly from the rest of the samples belonging to other categories, the remainder of the samples are mostly cluttered in one big heap having minimal separation between them. This shows that the KSLSH is not discriminative enough to separate the samples in the original Hamming space. On the contrary, as shown in Fig. 3b, t-SNE, when applied on the test set with the proposed MiLaN, leads to samples exhibiting very compact clusters. We also observe that since the deep metric space learns visual similarity, the clusters for “freeway” and “overpass”, which exhibit similar visual patterns, lie close to each other and yet far enough to have their own well-separated clusters in the 2D space.

Moreover, we have also analysed the impact of length of hash bits on retrieval performance. As seen in Fig. 5a, for both the KSLSH and the proposed MiLaN, the mAP for the top-20 retrieved images increases with an increase in the number of hash bits. However, the average precision curve for MiLaN associated to all K stays considerably above the KSLSH. This indicates that the proposed network efficiently maps semantic information into its discriminative hash codes with varying lengths, which the KSLSH fails to achieve. We also train MiLaN with different train:test splits and report the mAP@20 at $K=32$ in Fig. 5b. From Fig. 5b, one can see that the mAP obtained by the MiLaN by just using 30% training images is

TABLE III: mAP@20 and average retrieval time for the SVM, the KSLSH [2] and the proposed MiLaN for the AID archive.

Methods	mAP	Time (in ms)	# Hash Bits K					
			$K=16$		$K=24$		$K=32$	
			mAP	Time (in ms)	mAP	Time (in ms)	mAP	Time (in ms)
SVM	0.907	1124.7	-	-	-	-	-	-
KSLSH [2]	-	-	0.426	115.3	0.467	116.1	0.495	117.5
Our MiLaN	-	-	0.876	117.5	0.891	116	0.926	114.5

Fig. 5: Comparative analysis of the KSLSH and the MiLaN. mAP@20 curves of the KSLSH and the MiLaN on the UCMD for (a) different number of hash bits; and (b) different train:test ratio at $K = 32$. mAP@50 curves of the KSLSH and the MiLaN on the AID for (c) different number of hash bits; and (d) different number of top- k retrieved images at $K = 32$.

much higher than the mAP obtained by the KSLSH with 80% of total images as training images.

B. Results: AID Data Set

For the experiments conducted on the AID archive we split the images from each category with 60:40 train:test split-ratio. The results of this archive demonstrate similar trends as that of the UCMD. In summary, the MiLaN provides superior mAP@20 when compared to any other method. Table III shows that when $K = 16$ the mAP@20 of MiLaN is 45% higher than that of the KSLSH. Similar trend in mAP@20 is also observed between these two methods for higher value of K . In details, our proposed MiLaN exceeds the results of SVM by 1.9% when $K = 32$ and also reduces the retrieval time by almost a factor of 10. We also report the ablation studies conducted on the AID archive. As observed in Fig. 5c, when K increases the map@50 for MiLaN increases monotonically and outperforms the KSLSH for all values of K . Similarly, in Fig. 5d we notice that when the number of top- k retrieved images increases, the map@50 decreases slightly for MiLaN but quite significantly for the KSLSH.

V. CONCLUSION

In this letter we have introduced a metric-learning based deep hashing network for fast and accurate RS CBIR. The proposed network takes the intermediate representations of the images (from Inception Net pre-trained on ImageNet) and trains the network by means of different losses: i) a triplet loss that learns the target metric space; and ii) balancing and representation losses to efficiently learn binary hash codes. Due to the joint use of three losses, we learn a hash function which maps images to compact binary hash codes that can accurately describe complex information content of RS images. Experimental results obtained on two benchmark archives

demonstrate that the learned hash codes: (1) efficiently characterize the complex semantics in RS images with a relatively small annotated training set; and (2) leads to more accurate and high time-efficient similarity search. As a future development of this work, we plan to extend the proposed method to the framework of deep multi-code hashing problems, where each code corresponds to a primitive present in the image.

REFERENCES

- [1] M. Slaney and M. Casey, "Locality-sensitive hashing for finding nearest neighbors [lecture notes]," *IEEE Signal processing magazine*, vol. 25, no. 2, pp. 128–131, 2008.
- [2] B. Demir and L. Bruzzone, "Hashing-based scalable remote sensing image search and retrieval in large archives," *IEEE Transactions on Geoscience and Remote Sensing*, vol. 54, no. 2, pp. 892–904, 2016.
- [3] T. Reato, B. Demir, and L. Bruzzone, "An unsupervised multicode hashing method for accurate and scalable remote sensing image retrieval," *IEEE Geoscience and Remote Sensing Letters*, vol. 16, no. 2, pp. 276–280, 2019.
- [4] Y. Li, Y. Zhang, X. Huang, H. Zhu, and J. Ma, "Large-scale remote sensing image retrieval by deep hashing neural networks," *IEEE Transactions on Geoscience and Remote Sensing*, vol. 56, no. 2, pp. 950–965, 2018.
- [5] S. Roy, E. Sangineto, B. Demir, and N. Sebe, "Deep metric and hash-code learning for content-based retrieval of remote sensing images," in *IGARSS*. IEEE, 2018, pp. 4539–4542.
- [6] F. Schroff, D. Kalenichenko, and J. Philbin, "Facenet: A unified embedding for face recognition and clustering," in *CVPR*, 2015, pp. 815–823.
- [7] C. Szegedy, V. Vanhoucke, S. Ioffe, J. Shlens, and Z. Wojna, "Rethinking the inception architecture for computer vision," in *CVPR*, 2016.
- [8] H.-F. Yang, K. Lin, and C.-S. Chen, "Supervised learning of semantics-preserving hash via deep convolutional neural networks," *IEEE transactions on pattern analysis and machine intelligence*, vol. 40, no. 2, pp. 437–451, 2018.
- [9] O. E. Dai, B. Demir, B. Sankur, and L. Bruzzone, "A novel system for content-based retrieval of single and multi-label high-dimensional remote sensing images," *IEEE Journal of Selected Topics in Applied Earth Observations and Remote Sensing*, vol. 11, no. 7, pp. 2473–2490, 2018.
- [10] G.-S. Xia, J. Hu, F. Hu, B. Shi, X. Bai, Y. Zhong, L. Zhang, and X. Lu, "Aid: A benchmark data set for performance evaluation of aerial scene classification," *IEEE Transactions on Geoscience and Remote Sensing*, vol. 55, no. 7, pp. 3965–3981, 2017.